Tuning the Size of Silver Nanodisks with Similar Aspect Ratios: Synthesis and Optical Properties

Mathieu Maillard,[†] Suzanne Giorgio,[‡] and Marie-Paule Pileni*[,†]

LM2N, URA CNRS 1662, Université Pierre et Marie Curie, BP 52, 4 Place Jussieu, 75252 Paris Cedex 05, France, and CRMC2-CNRS, Campus de Luminy, Case 913, 13288 Marseille Cedex 9, France

Received: November 1, 2002

This paper describes the first method for making nanodisks having similar aspect ratios and differing by their size. Flat, single-crystal silver nanodisks in equilibrium with spheres are produced using colloidal solutions. The nanodisk size is tuned by the relative amount of reducing agent involved in the synthesis whereas their aspect ratios remain the same order of magnitude. The 3D nanodisk shape is determined by transmission electronic microscopy using the weak-beam dark-field technique. These nanodisks characterized by such anisotropic shapes exhibit several plasmon resonance modes observed in the UV−visible range.

I. Introduction

Nanomaterials are now an important research field, especially because their properties can be tuned by a single parameter. The most famous example is the size-tunable band gap of semiconductor nanocrystals.[1] More recently, such size dependency has been obtained with other materials and other properties such as the Curie temperature from magnetic nanoparticles[2] or the Coulomb blockade from metals.[3] An alternative way to introduce such an adjustable property is to control the shape anisotropy. Thus, metallic nanorods such as gold[4] or silver[5] exhibit anisotropic optical properties that are directly related to their aspect ratio. In the same way, CdSe nanorods' luminescence[6] and maghemite magnetic properties[7] and nickel[8] or cobalt[9] nanorods are also markedly affected by their shape.

In this paper, we describe the first size-tunable silver nanodisk synthesis at a constant aspect ratio. In equilibrium with these nanodisks, spherical polycrystalline particles are produced. The particle size is tuned by the experimental conditions. The absorption spectra of assemblies of spheres and nanodisks exhibit several surface plasmon resonances related to the nanocrystal shape and size.

II. Experimental Section

Sodium di(2-ethyl-hexyl)sulfosuccinate (Na(AOT)), isooctane, hydrazine, and dodecanethiol were from Sigma, Fluka, Prolabo (France), and Janssen chemicals, respectively. The materials were used without further purification.

Transmission electron micrographs (TEM) were obtained using a JEOL 100CXII operating at 100 keV.

III. Results and Discussion

III.1. Synthesis and Characterization. Silver di(2-ethyl-hexyl)sulfosuccinate, Ag(AOT), is made as described previously.[10] Colloidal silver particles are obtained by mixing two solutions. The first one is a reverse micelle solution made of 60% 0.1 M Ag(AOT) and 40% 0.1 M Na(AOT) solubilized in isooctane. The water content, $w = [H_2O]/[AOT]$, is kept at 2. The second one is 0.1 M Na(AOT) in isooctane, with water replaced by hydrazine (N_2H_4). The overall hydrazine concentration varies from 0.5 to 1.66 M, and its content, defined as $y = [N_2H_4]/[AOT]$, varies from 5 to 16.6. The solution, stirred for 20 min, becomes opalescent because a phase transition takes place: reverse micelles are no longer formed. The two solutions are mixed together, and a dark color quickly appears. The solution is then diluted 100 times in 0.1 M Na(AOT) solution and subjected to ultrasound for 10 min. The color of the solution depends on the initial synthesis conditions, from red for the lowest reducing agent ratio to green and gray for the highest (Figure 1). The solution remains stable for several days. A drop of solution is deposited on a carbon grid covered by amorphous carbon, and nanocrystals are observed by TEM. However, a rapid transformation under the electron beam is observed, with the formation of smaller particles having a strong contrast in the neighborhood of the larger ones. Such behavior is observed for all of the samples, even at low electron doses and low magnification. Indeed, small particles are always more stable when they are stabilized, for example, by epitaxial orientation on a crystalline substrate.[11,12] To perform a quantitative structural study of the nanocrystals produced at various reducing agent concentrations, dodecanethiol (20μL/mL) is added to the solution, and after 3 h, it is centrifuged. The coated nanocrystals are then redispersed in ethanol. After a 10-min centrifugation

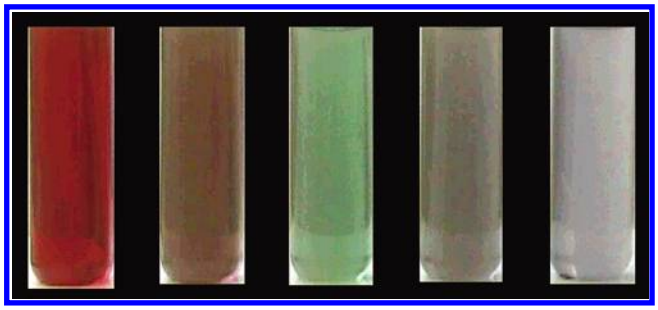

Figure 1. Solutions of nanocrystals dispersed in reverse micelles and obtained at various hydrazine concentrations. ($y = [N_2H_4]/[AOT] =$ 4.9, 5.8, 6.6, 8.2, and 12.3.)

* To whom correspondence should be addressed: E-mail: pileni@sri.jussieu.fr. Web: http://www.sri.jussieu.fr.
[†] Université Pierre et Marie Curie.
[‡] Campus de Luminy.

10.1021/jp022357q CCC: $25.00
Published on Web 02/21/2003

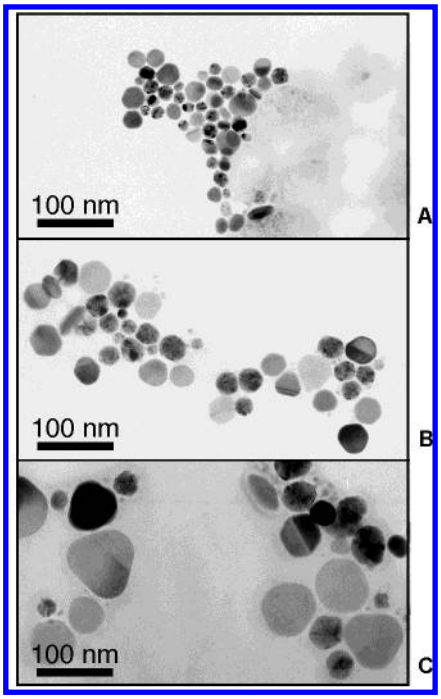

Figure 2. Silver nanocrystals as observed by TEM at various hydrazine contents: (A) $y = 5.35$, (B) $y = 6.6$, and (C) $y = 8.2$.

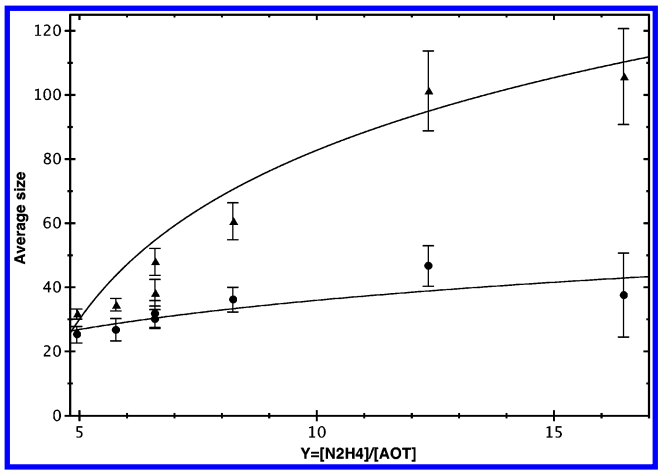

Figure 3. Dependence of the average size of the faceted particles (▲) and spheres (●) on the hydrazine content. The solid line is an effective fit.

at 5000 rpm, the solvent is removed, and the particles at the bottom of the vessel are redispersed in 0.1 M Na(AOT) in isooctane. Particles are now found to be stable under the electron beam. This is probably due to the fact that the strong binding of thiododecane to the metal surface induces a decrease in the surface tension of nanocrystal faces, preventing the destructive heating effect due to the electron beam. A drop of the solution containing the nanoparticles is deposited on a copper grid and observed by TEM. Figure 2 shows TEM images obtained at the end of the procedure and corresponding to syntheses made at various hydrazine contents, y. Under all experimental conditions, spheres and hexagons are produced. The average size of hexagons (defined as the distance between two parallel faces) and spheres increases with increasing hydrazine content, y, and size distribution. Figure 3 shows a more pronounced increase in the size of hexagons than in that of spheres with y. Similar behavior is found by taking into account the number of atoms involved in hexagons and spheres. Around 100 particles are counted to determine the average particle size.

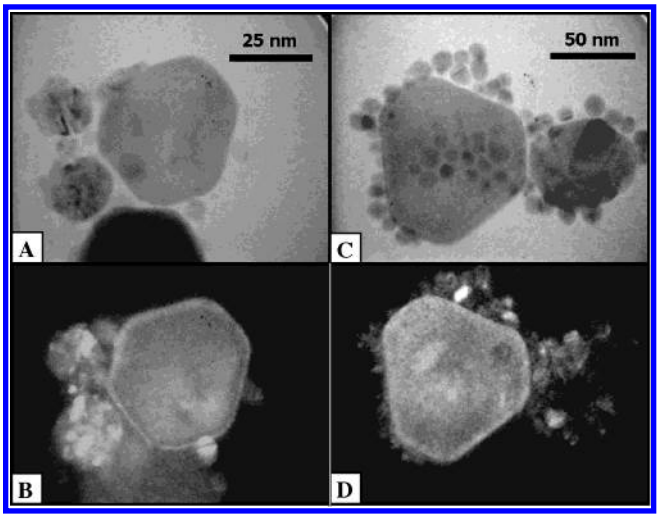

Figure 4. Bright (A, C) and dark (B, D) fields of TEM pictures of flat nanocrystals obtained at various hydrazine contents ($y = 6.6$ for A and B; $y = 16.5$ for C and D).

Structural studies of these nanocrystals are performed on a very large number of samples through various approaches: From the electron diffraction (ED) pattern of the overall nanocrystals, the lattice parameter is found to be $a = 4.17 \pm 0.09$ Å, which is in good agreement with that of the bulk silver fcc structure ($a_0 = 4.08$ Å). The ED pattern of an isolated hexagon shows several well-defined sharp spots in six-fold symmetry corresponding to a fcc single crystal oriented toward the [111] direction.[13] This is obtained for various nanodisk sizes.

To determine the crystallinity of the spheres and hexagons, the TEM images on the same coated particles in bright (Figure 4A and C) and dark (Figure 4B and 4D) fields are compared. In bright field, the TEM images (Figure 4A and C) show the formation of more or less regular hexagons with uniform contrasts, indicating single-crystal nanoparticles. Spherical nanoparticles, differing by their sizes, are mixed with the faceted ones. They are characterized by various contrasts indicating several crystalline defects. This is confirmed by dark-field imaging of the same nanoparticles (i.e., using only part of the diffracted beam instead of the central beam for the image formation). Figure 4B and D show very bright faceted particles, indicating a strongly diffracting crystal and, consequently, a well-crystallized nanoparticle. This clearly shows that hexagons are mainly single crystals. This confirms the electron diffraction data on a single particle described above. Conversely, spherical particles appear with many twins defects. Their contrast varies, indicating polycrystalline objects. They are the result of an aggregation of tetrahedral seeds generating five-fold symmetry and more polycrystalline particles.[14,15]

The shape of hexagon nanocrystals is determined by TEM using WBDF imaging.[16,17] When the sample is tilted by $\Delta\theta$ from the Bragg orientation, a set of fringes of equal thickness are formed, with the distance between the fringes given by the equation $i = 1/(g_{(220)}tg\alpha\Delta\theta)$, where α and $g_{(220)}$ are the angle between the lateral face and the substrate and the reciprocal vector corresponding to the (220) reflections, respectively. From this, the faces normal to the electron beam appear to have uniform intensity whereas faces making an angle with the electron beam have bright and dark fringes. Figure 5A, C, and E show, for various nanocrystal sizes, a homogeneous surface surrounded by fringes. The profile plots corresponding to those of nanocrystals (Figure 5B, D, F, and H) clearly show the two different lateral faces that are consistent with (100) and (111) faces, with respective angles of 54 and 71° with regard to the

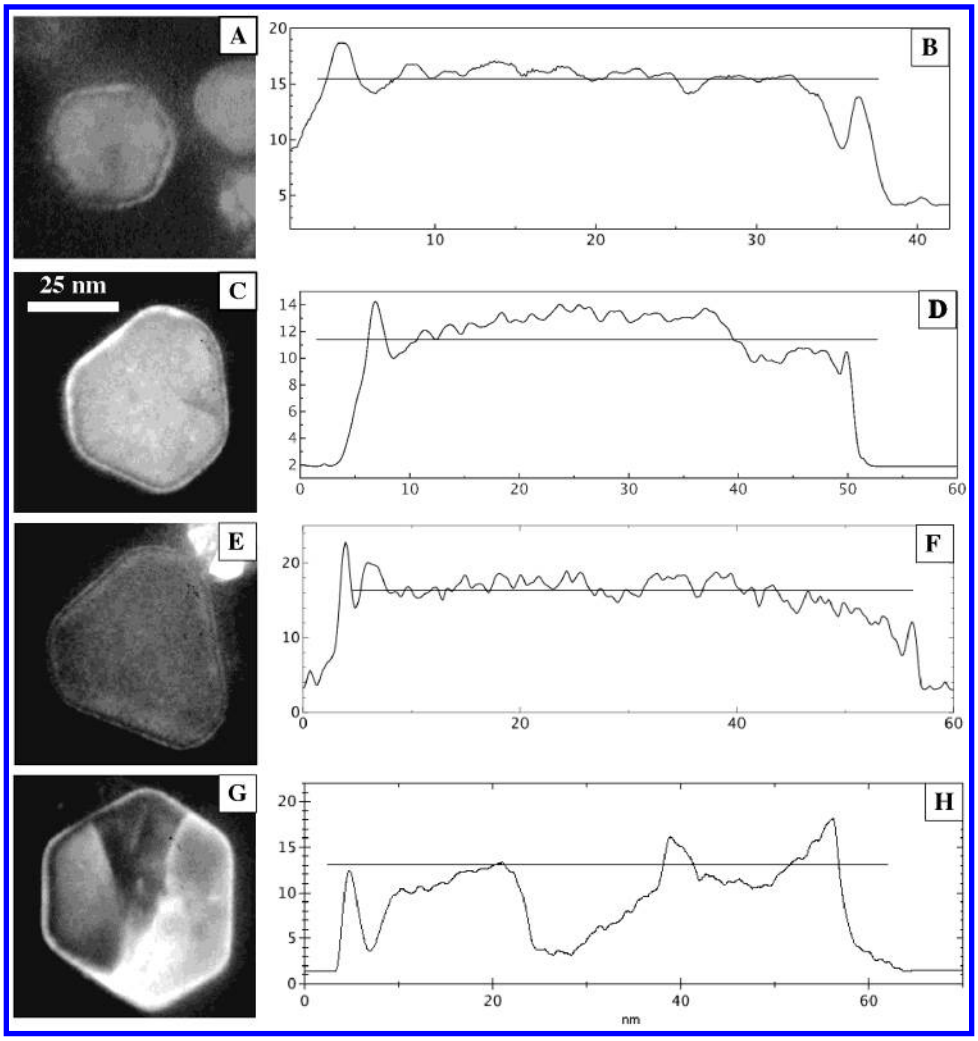

Figure 5. (A, C, E, and G) Dark-field TEM picture of single nanodisks differing in size. Tilted nanocrystals in dark field using the (220) reflection at a low tilt angle (3°). (B, D, F, and H) Intensity variation along the particle diameter (A, C, E, and G).

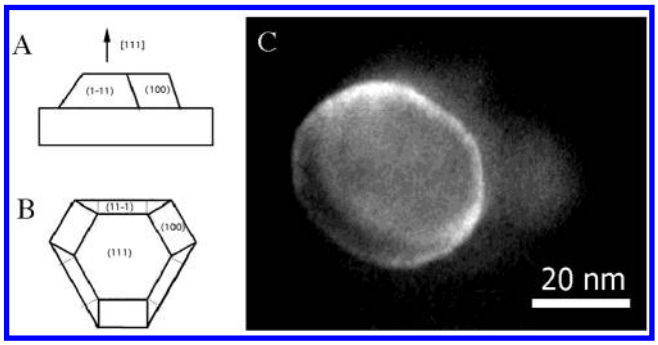

Figure 6. Profile view (A) and top view (B) of a truncated crystal (111) oriented on the substrate. (C) Silver nanodisk observed by TEM under dark field at a high tilt angle.

substrate. Figure 5G shows a rough surface with no regular profile (Figure 5H). This is due to a crystalline defect, inducing a slight mismatch of the crystalline orientation with the electron beam. From these data, we conclude that faceted particles appear as flat single crystals with two (111) faces at the top and the bottom, limited at the edges by three other (111) faces and at the corners by more or less extended (100) faces. Hence, flat pseudo-hexagonal nanocrystals are produced (Figure 6A and B). From a larger tilt angle under dark-field imaging (Figure 6C), the flat hexagonal shape of the nanocrystals is more pronounced. From the profile plots made for a rather large number of particles, we conclude that these flat particles are characterized by an aspect ratio between 4 and 5.5.

The structural study performed with samples made at various *y* values clearly indicates that they drastically differ by their sizes whereas there is little change in the aspect ratio.

III.2. Optical Properties. From structural studies, it is obvious that single-crystal nanodisks and polycrystalline nanospheres are simultaneously produced. By increasing the hydrazine content, *y*, their sizes increase, inducing drastic changes in the optical properties (Figure 1). Figure 7 shows the absorption spectra of a solution containing both nanodisks and spheres obtained at various particle sizes (i.e., various *y* values). Several peaks are observed and attributed to surface plasmon resonances (SPR) characteristic of noble-metal nanoparticles.[18]

The increase in the size of the silver nanospheres and nanodisks induces a red shift of the SPR peaks. Figure 7 and Table 1 show that the high-energy peak (peak 1) does not drastically change with the particle size, the mid-energy peak (peak 2) slightly shifts from 2.91 to 2.68 eV, and the low-energy peak (peak 3) shifts from 2.57 to 1.73 eV. The energy difference between the high- and low-energy peaks is plotted as a function of the particle size (Figure 8). A continuous splitting with the particle size is clearly observed.

Whatever the hydrazine content is, these peaks are shifted and broadened by dodecanethiol addition to the solution. This well-known phenomenon is attributed to the thiol group binding to the metal surface.[19,20] As an example, Figure 9 shows

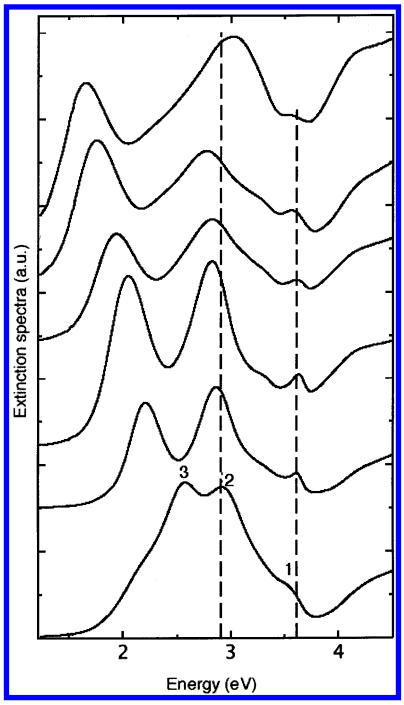

Figure 7. Absorption spectra obtained with the solution containing particles of different sizes. Bottom to top: $D = 30$, 35, 51, 61, 100, and 107 nm.

TABLE 1: SPR Peak Positions as a Function of the Reducing Agent Content Y and the Size of the Nanodisks and Spheres before Capping the Particles with Thiododecane

Y	hexagon size	sphere size	peak 1	peak 2	peak 3	ΔE (eV)
4.9	31.7	25.2	3.56	2.91	2.57	0.99
5.8	34.6	26.8	3.56	2.96	2.51	1.05
6.6	47.9	31.7	3.61	2.86	2.2	1.41
8.2	60.6	36.2	3.63	2.83	2.05	1.58
12.3	101.3	46.7	3.57	2.77	1.75	1.82
16.5	105.7	37.6	3.59	2.68	1.73	1.86

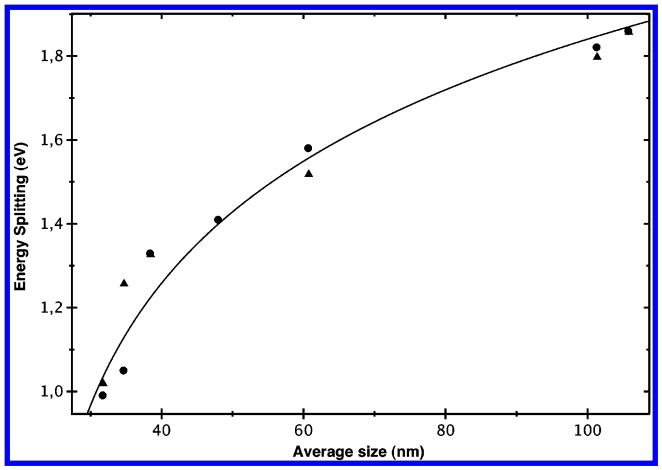

Figure 8. Dependence of the energy splitting on the nanodisk size before (●) and after (▲) adding thiododecane. The solid line is an effective fit.

absorption spectra before (solid line) and after (dashed line) coating for a solution containing spherical nanocrystals and nanodisks having average sizes of 35 and 65 nm, respectively. Note a strong shift for the lowest-energy peak whereas the others remain in the same energy range (Table 2). The energy difference between the high- and low-energy peaks is similar to that obtained before coating (Figure 8). This confirms that particles retain their structure after coating.

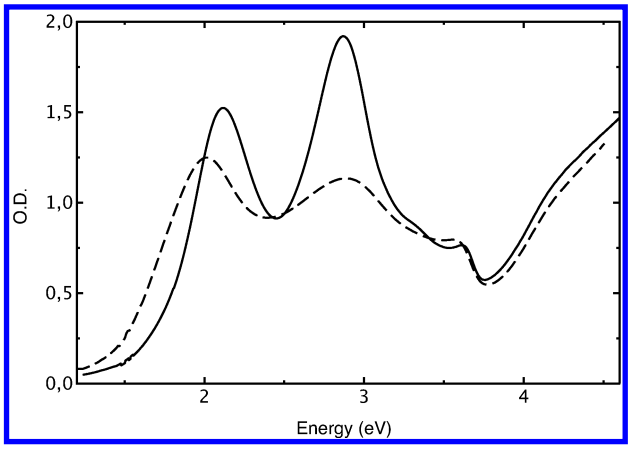

Figure 9. Absorption spectra obtained before (—) and after (– –) adding thiododecane to a nanoparticle solution obtained with a hydrazine content of $y = 6.6$.

TABLE 2: SPR Peak Positions as a Function of the Reducing Agent Content Y and the Size of the Nanodisks and Spheres after Capping the Particles with Thiododecane.

Y	hexagon size	sphere size	peak 1	peak 2	peak 3	ΔE (eV)
4.9	31.7	25.2	3.58	2.96	2.53	1.05
5.8	34.6	26.8	3.56	3.02	2.35	1.21
6.6	47.9	31.7	3.62	2.94	2.24	1.38
8.2	60.6	36.2	3.62	2.89	2.01	1.61
12.3	101.3	46.7	3.5	2.82	1.66	1.84
16.5	105.7	37.6	3.55	2.67	1.7	1.85

The attribution of these various SPR peaks is not very easy because no analytic solutions are available for such truncated disk like particles. However, by taking into account data from the literature, it is possible to assign most of these peaks. We have to keep in mind that they are due to a mixture of silver nanospheres and nanodisks.

Let us first consider the silver nanospheres with an average diameter varying from 25 to 40 nm. The SPR of silver spherical nanocrystals is characterized by a single resonance centered close to 3 eV.[19] This is close to the mid-peak (peak 2). The slight shift of this peak to lower energy upon increasing the particle size from 25 to 40 nm is due to the fact that the particle size is no longer small compared to the wavelength and the applied electric field is not homogeneous.[18] This induces retardation effects and allows us to attribute the mid-energy peak to spherical particles. This is confirmed by the fact that its position does not markedly change with the coating (Table 2).

The change in optical properties with particle size must be related to the fact that we are dealing with anisotropic particles. It is well known that particle shape drastically modifies the extinction spectrum. For a flattened ellipsoid-shaped nanocrystal, two plasmon modes are observed, which are called longitudinal and transverse modes and correspond to the polarization along the long and the short axes of the ellipsoid. The energy splitting between these two plasmon modes is directly related to the aspect ratio, and the SPR positions for such a flattened ellipsoid are below and above the sphere SPR position. Taking into account these data, the high- (peak 1) and low-energy peak (peak 3) are attributed to the anisotropy of the nanoparticles (i.e, to the nanodisks). This is confirmed by the fact that the coating induces a large shift of the low-energy peak that is attributed to the longitudinal mode (Table 2). Because the disk aspect ratio remains in the same order of magnitude (4.4−5), the red shift of the low-energy peak is related only to the increase in the disk size because of retardation effects. This effect is more important because the increase in the particle size is more

pronounced for nanodisks (30−100 nm) than for spheres (25−40 nm). This is in agreement with the macroscopic observation of a continuous color change from red to green and then to gray by increasing the particle size (Figure 1).

Hence, SPR peaks at high and low energy are attributed to the nanodisk transverse and longitudinal modes whereas the mid-peak is due to the spheres. Additional SPR peaks cannot be excluded because the presence of four plasmon modes has been demonstrated for flat triangles.[22−24] Between the lowest- and the highest-energy peaks, other SPR peaks may exist but would be screened by the spheres' absorption. This could explain the presence of a shoulder around 3.2 eV when the particle size increases. At the present state of the art, it is rather difficult to formulate other hypotheses.

IV. Conclusions

A new synthesis for producing large silver spheres and nanodisks has been described. The 3D disk shape resembles pyramids with an extended truncation on the top. Their size is controlled between 30 and 100 nm by the relative amount of reducing agent. Their absorption spectra show many absorption peaks that are attributed to different surface plasmon resonance modes. This optical anisotropy is related to the nanodisk's 3D shape. The energy position of these peaks is related to the particle size because of retardation effects. Hence, it is possible to tune the optical absorption by a simple chemical procedure.

It is clear that these results are the first steps in a longer study to identify more precisely the various SPR peaks. Thus, the way to produce nanodisks selectively with a small size and a narrow shape distribution needs to be improved. This would allow us to obtain the nanodisks' specific absorption spectra when they are dispersed in solution and differ by their sizes. Of course, optical studies of isolated particles by SNOM would be one way to solve this problem. At least numerical simulations taking into account the particle shape and size, using the discrete dipole approximation (DDA),[24] for example, would provide useful answers with respect to these effects.

Acknowledgment. We thank Dr. C. Henry (CRMC2, Marseille), Dr. P. Melinon (LP-Lyon) and Dr. F. Vallée (CPMOH, Bordeaux) for fruitful discussions on optical properties and aggregate stability and Dr. F. Warmont for carrying out part of the bright-field TEM imaging.

References and Notes

(1) Brus, L. E. *J. Chem. Phys.* **1983**, *79*, 5566. Bruchez, M., Jr.; Moronne, M. P. G., Weiss, S.; Alivisatos, P. A. *Science (Washington, D.C.)* **1998**, *281*, 2013.

(2) Ngo, A. T.; Bonville, P.; Pileni, M. P. *J. Appl. Phys*. **2001**, *89*, 3370.

(3) Wang, B.; Wang, H.; Li, H.; Zeng, C.; Hou, J. G.; Xiao, X. *Phys. Rev. B* **2000**, *63*, 035403.

(4) Yu, Y. Y.; Chang, S. S.; Lee, C. L.; Wang, C. R. C. *J. Phys. Chem. B* **1997**, *101*, 1588.

(5) Jana, N. R.; Gearheart, L.; Murphy, C. J. *Chem. Commun.* **2001**, 617.

(6) Hu, J.; Li, L.; Yang, W.; Manna, L.; Wang, L.; Alivisatos, A. P. *Science (Washington, D.C.)* **2001**, *292*, 2060.

(7) Ngo, A. T.; Pileni, M. P. *J. Appl. Phys.*, in press.

(8) Cordente, N.; Respaud, M.; Senocq, F.; Casanove, M. J.; Amiens, C.; Chaudret, B. *Nano Lett.* **2001**, *1*, 565.

(9) Puntes, V. F.; Kroshnan, K. M.; Alivisatos, A. P. *Science (Washington, D.C.)* **2001**, *291*, 2115.

(10) Petit, C.; Lixon, P.; Pileni, M. P. *J. Phys. Chem.* **1993**, *97*, 12974.

(11) Ajayan, P. M.; Marks, L. D. *Nature (London)* **1989**, *338*, 139. Ajayan, P. M.; Marks, L. D. *Phys Rev. Lett.* **1989**, *63*, 279.

(12) Giorgio, S.; Henry, C. R.; Chapon, C.; Nihoul, G.; Penisson, J. M. *Ultramicroscopy* **1991**, *38*, 1−12.

(13) Maillard, M.; Giorgio, S.; Pileni, M. P. *Adv. Mater.* **2002**, *14*, 1084.

(14) Pileni, M. P. *Langmuir* **2001**, *27*, 74−78.

(15) Courty, A.; Lisiecki, I.; Pileni, M. P. *J. Chem. Phys*. **2002**, *116*, 8074−8078.

(16) Yacaman, J.; Ocana, T. *Phys. Status Solidi A* **1977**, *42*, 571.

(17) Giorgio, S.; Graoui, H.; Chapon, C.; Henry, C. R. *Cryst. Res. Technol.* **1998**, *33*, 1061.

(18) Kreibig, U.; Vollmer, M. *Optical Properties of Metal Clusters;* Springer Publishing: New York, 1993.

(19) Taleb, A.; Petit, C.; Pileni, M. P. *J. Phys. Chem. B* **1998**, *102*, 2214.

(20) Persoon, B. N. *J. Surf. Sci.* **1993**, *281*, 153.

(21) Kottmann, J. P.; Martin, O. J. F.; Smith, D. R.; Schultz, S. *Phys. Rev. B* **2001**, *64*, 235402.

(22) Jin, R.; Cao, Y.; Mirkin, C. A.; Kelly, K. L.; Schatz, G. C.; Zheng, J. G.; *Science (Washington, D.C.)* **2001**, *294*, 1901.

(23) Yang, W. Y.; Schatz, G. C.; Van Duyne, R. P. *J. Chem. Phys.* **1995**, *103*, 869−875.

(24) Schatz, G. C. *Theor. Chem*. **2001**, *573*, 73−80.